

Article www.acsabm.org

Highly Aligned Electrospun Collagen/Polycaprolactone Surgical Sutures with Sustained Release of Growth Factors for Wound Regeneration

Jinyu Hu, Yi Song, Cuiyun Zhang, Wen Huang, Anqi Chen, Huacheng He, Susu Zhang, Yanxin Chen, Chaodong Tu, Jianhui Liu, Xuan Xuan, Yung Chang, Jie Zheng,* and Jiang Wu*



Cite This: ACS Appl. Bio Mater. 2020. 3, 965-976



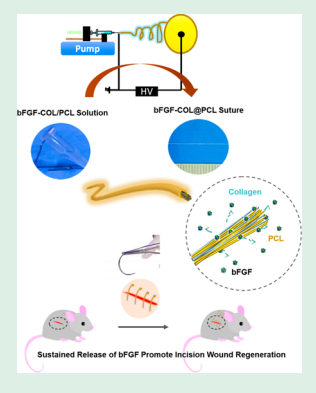
ACCESS

III Metrics & More

Article Recommendations

Supporting Information

ABSTRACT: Development of biocompatible and bioactive drug-loaded sutures is considered as an effective but challenging strategy for the wound healing process by delivering biological drugs (e.g., antibiotics) or growth factors (e.g., bFGF) at the surgical wound sites. Conventional offline suture strategies often lead to fast and uncontrollable release of drugs at wound sites, rendering wound healing to become a longer and painful process for patients. Herein, we propose an online suture strategy to fabricate electrospun polycaprolactone (PCL) fibrous yarns, incorporated with both collagen (COL) and bFGF, to produce bFGF-COL@PCL sutures. Upon demonstrating the welloriented and aligned fibrous microstructure, high mechanical properties, and controlled release of bFGF from bFGF-COL@PCL sutures in vitro, we then applied bFGF-COL@PCL sutures to an incision wound healing mouse model in vivo. Further in vivo study showed that as compared to the commercialized Vicryl suture, bFGF-COL@PCL sutures significantly promoted the wound healing at different stages by accelerating granulation tissue formation, collagen deposition, and reepithelialization. The enhanced wound healing efficiency of bFGF-COL@PCL sutures is likely



attributed to two synergistic factors: (i) the well-oriented nanofibrous structure reduces tissue drag to minimize their trauma and (ii) the presence of both collagen and bFGF enhances the basement membrane (BM) reconstruction, cell proliferation, and angiogenesis. This work demonstrates an effective suture strategy and system for surgical suture applications.

KEYWORDS: suture, sustained release, growth factor, electrospinning, wound healing

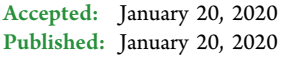
1. INTRODUCTION

Surgical regeneration of connective tissues such as vascular,¹ tendons,² and viable tissues³ remains a long-standing clinical challenge, primarily because insufficient treatment, repair, and even failure of injured sites by insufficient regeneration often cause unwanted inflammatory, pathological thrombosis, and progressive occlusion.^{4,5} Drug-eluting surgical sutures have been commonly used as delivery depots for antibiotics, antiinflammatory, and anesthetics at surgical sites. While adding chemical drug have repaired the injured to some extents, they are still limited by insufficiently regulating of the initial subsequent healing process. To overcome these limitations, the incorporation of growth factors and stem cells into the suture could offer a more bioactive and effective strategy to improve the healing of wounds and injuries.^{7,8} Particularly, the sustained release of growth factors such as transforming growth factor β (TGF β), vascular endothelial growth factor (VEGF), platelet-derived growth factor (PDGF), and basic fibroblast growth factor (bFGF) to wound sites is essential for tissue regeneration due to the their biological functionality. 9-12 Among them, bFGF (also known as FGF2), as a mitogenic and angiogenic factor, 13 has been discovered to play a significant role in different physiological and pathological processes,

including promoting wound healing and reducing scar formation. ^{14,15} So, bFGF is used as a model growth factor in sutures to promote surgical regeneration and an antiscar effect.

Since surgical sutures often function as delivery depots and mechanical support to load bioactive molecules (e.g., drugs and growth factors), different drug-loading strategies, including mixing, adsorption, coating, and swelling, have been proposed. Among them, drug-coated suture is a simple and straightforward strategy that offer high-mechanical strength, biodegradability, and low tissue responsiveness but suffers from low drug-loading capacity and burst drug-releasing kinetics, presumably because almost all coated drugs are exclusively exposed to the biological environments. 16,17 To overcome the low surface-coating limit, electrospun fibers containing microor nanosized fibrous structures present high surface-to-area ratios, ^{18–24} allowing one to achieve high drug loading and controlled release. ^{25,26} A number of studies have reported that

Received: October 29, 2019 Accepted: January 20, 2020





collagen-loaded electrospun nanofibers are well used as tissue engineering scaffolds to mimic extracellular matrix (ECM) for promoting tissue regeneration, cell adhesion, fibroblast migration, and vascularization. However, challenges still remain. Most of electrospun fibers exhibited poor mechanical properties due to randomly oriented fibers, which greatly limit their uses as strong surgical sutures. 25,29

To circumvent these above-mentioned limitations, we fabricated multifunctional aligned electrospun fibrous sutures bFGF-COL@PCL, made of biodegradable polycaprolactone (PCL) and collagen (COL) and loaded with bFGF, to achieve both mechanical strength and controllable drug-loading/ release. An in-house rotating edge-sharpened disc collector was developed to produce highly aligned nanofibers and bundled nanofiber yarns as surgical sutures, during which bFGF was first loaded into water solution to obtain its biofunctionality, then mixed with collagen-PCL solution following by coelectrospinning with PCL. The resultant bFGF-COL@PCL sutures with continuously aligned PCL fibers exhibited the stronger mechanical properties than those sutures with randomly oriented fibers. The morphology, microstructure, mechanical properties, and controlled release of bFGF from the bFGF-COL@PCL sutures were systematically tested to reveal its structure-function relationship. Finally, bFGF-COL@PCL sutures were applied to an acute incision cutaneous animal model and demonstrated their promotion effects for wound healing.

2. MATERIALS AND METHODS

2.1. Materials. Basic fibroblast growth factor (bFGF) (the Key Laboratory of Biotechnology and Pharmaceutical Engineering, Wenzhou Medical University, China). Polycaprolactone (PCL, MW = 80 000) was purchased from Sigma-Aldrich Chemical Company. 1,1,1,3,3,3-Hexafluoro-2-propanol (HFIP) was purchased from Aladdin. The collagen and specific bFGF enzyme-linked immunosorbent assay kits were purchased from Shang Westang Biotech Co. Ltd. Bovine serum albumin (BSA) was obtained from Beyotime. The H&E staining kit, Masson's trichrome staining kit, AB-PAS (Alcian Blue-Periodic Acid Schiff) staining kit, and Sirius red staining kit were purchased from Solarbio Sciences & Technology Co. Ltd. (Beijing, China). Primary antibodies anti wide spectrum cytokeratin (ab9377), CD31 (ab28364), tumor necrosis factor alpha (TNF- α), Ki67 (ab15580) and secondary antibodies including goat antirabbit IgG Alexa Fluor 647 (ab150075) and goat antirabbit IgG Alexa Fluor 488 (ab150077) were purchased from Abcam (CA, U.K.). Goat antirabbit lgG (H&L) HRP conjugated antibody was purchased from Biovision.

2.2. Preparation of Electrospinning of COL@PCL Composite Fibrous Scaffold Containing bFGF. Drug-carrying polymer solution was compounded by the embedding method using PCL as the main scaffold. In brief, 226.3 mg of collagen was first dissolved in 6.75 mL of HFIP, following addition of 250 μ L of bFGF water solution including 700 μg of bFGF. The whole system was placed in an ice water bath overnight for complete bFGF loading. Then 0.68 g of PCL (MW = 80 000) was added to the mixed solution and kept stirring for 3 h until it was mixed thoroughly. An electrospinning device (YFSP-GIII, Tianjin Yunfan Technology Co. Ltd.) was used to prepare bFGF-COL@PCL sutures. Polymer solution was placed in a 10 mL syringe, and a fine needle with an inner diameter of 0.6 mm was selected to spin. The output voltage was controlled between 11 and 12 kV, the distance between the spinning needle and the receiver was 12-13 cm, the driving speed of the syringe pump was set at 0.0008 mm/s, and the receiving time of the receiver is controlled within 5-8 min. Under these conditions, the spinning thickness formed on the turntable receiver was most uniform, and a bFGF-COL@PCL ultrafine fiber with an outer diameter of 0.1 mm was obtained.

- **2.3. Fiber Morphology.** The morphology and structure of suture were confirmed by SEM (Japan S Hitachi Company). Sutures (2 cm) from the groups of PCL, COL@PCL, and bFGF-COL@PCL were pasted in the copperplate for pumpdown and gold spray with the sputter coater. Finally, the microstructure of the fibrous scaffold containing bFGF particles was observed and photographed under different magnifications.
- **2.4. Protein Encapsulation and Release.** Cy5 labeled bFGF was fabricated through following procedure. Cy-5 fluorescent dyes (10 mg, Thermofisher Scientific) dissolved in 1 mL of dimethyl sulfoxide (DMSO) and 1 mg of bFGF dissolved in 1 mL of PBS are mixed together and reacted for 3 h. Unreacted Cy-5 was dialyzed through a 7 kDa dialysis bag (Solarbio, China), and then the reaction solution was frozen at $-80\,^{\circ}\mathrm{C}$ and lyophilized by a vacuum freezedryer for 24 h. This Cy5-bFGF was used to evaluate the distribution of the proteins in the suture.

The growth factor release capacity of bFGF-COL@PCL suture was measured in a period of 20 days. bFGF-COL@PCL suture (5 cm) was immersed in solution (500 μ L) under the conditions of 37 $^{\circ}$ C and at different time points (6 h, 12 h, 1 day, 2 days, 3 days, 4 days, 5 days, 6 days, 7 days, 8 days, 9 days, 10 days, 11 days, 12 days, 13 days, 14 days, 15 days, 16 days, 17 days, 18 days, 19 days, 20 days); all solution (500 μ L) was removed and replaced with fresh solution (500 μ L). Obtained solutions were then placed in the heat preservation box to collect released bFGF, and these collected samples were stored in $-20~^{\circ}\text{C}$ until analysis. The samples were tested by enzyme-linked immunosorbent assay (ELISA, Westang system, Shanghai, China). The absorbance of bFGF at 450 nm was measured by the multifunctional SpectraMax M2e (Shanghai Beauty Molecular Instrument Co., Ltd.). The cumulative release rate was calculated, and the release curve was plotted based on the conversion of the calibration curve.

- **2.5. Mechanical Properties.** Tensile tests were performed with testing machine (Instron Limited of the United States) at 15 m/h at room temperature. Sutures with lengths of 20–30 mm were tested. Single tensile stress-dependent tests, tensile modulus, maximum tensile stress, and cycle tensile tests were obtained from the stress and strain curve.
- 2.6. Animal Model. Twenty-four healthy male C57BL/6 mice with a body weight of about 20 g were provided by the Laboratory Animals Center of Wenzhou University. The mice were anesthetized, their dorsal hair was shaved, and 1 cm long incisions were made with a sterile blade on both sides of the mice dorsal line. Then these mice were divided into four groups randomly. The four groups were treated with PCL suture, COL@PCL suture, bFGF-COL@PCL suture, and Vicryl absorbable suture, respectively (6 animals/12 wound per group), after sterilization of sutures under UV light for 2 h in 4 °C. Thereafter, the mice were housed in cages and observed daily throughout the course of the experiment. The body weight of each mouse and the images of each wound were collected on days 0, 3, 5, 7, 10, and 13, respectively. Besides, we performed statistical analysis of the wounds using software. On days 5 or 13, a dermatoscope was used to observe subcutaneous blood vessels and histological evaluation was performed after euthanasia and skin tissue harvest. The whole animal experiment was approved by the Animal Experimentation Ethics Committee of Wenzhou Medical University and was carried out under the guidelines of the National Institutes of Health Guide Concerning the Care and Use of Laboratory Animals.
- **2.7. Histological Analysis.** Six pieces of wound tissue were randomly selected and harvested from each group, respectively, on days 5 and 13. After fixation with 4% paraformaldehyde for 24 h at 4 $^{\circ}$ C, followed by gradient dehydration, the samples were embedded into paraffin. Sections with a thickness of 5 μ m were prepared using a paraffin slicing machine (Thermo Fisher) and were then put into a 60 $^{\circ}$ C drying oven for 6 h following histological staining.
- **2.8. Hematoxylin-Eosin Staining.** Tissue sections were dewaxed in xylene for 30 min and underwent gradient hydration. The cell nucleus of tissue sections was stained with hematoxylin, and excess background removal was done through PBS rinsing for 3 min. Then samples were stained with eosin for 2.5 min and rinsed with distilled

ACS Applied Bio Materials www.acsabm.org

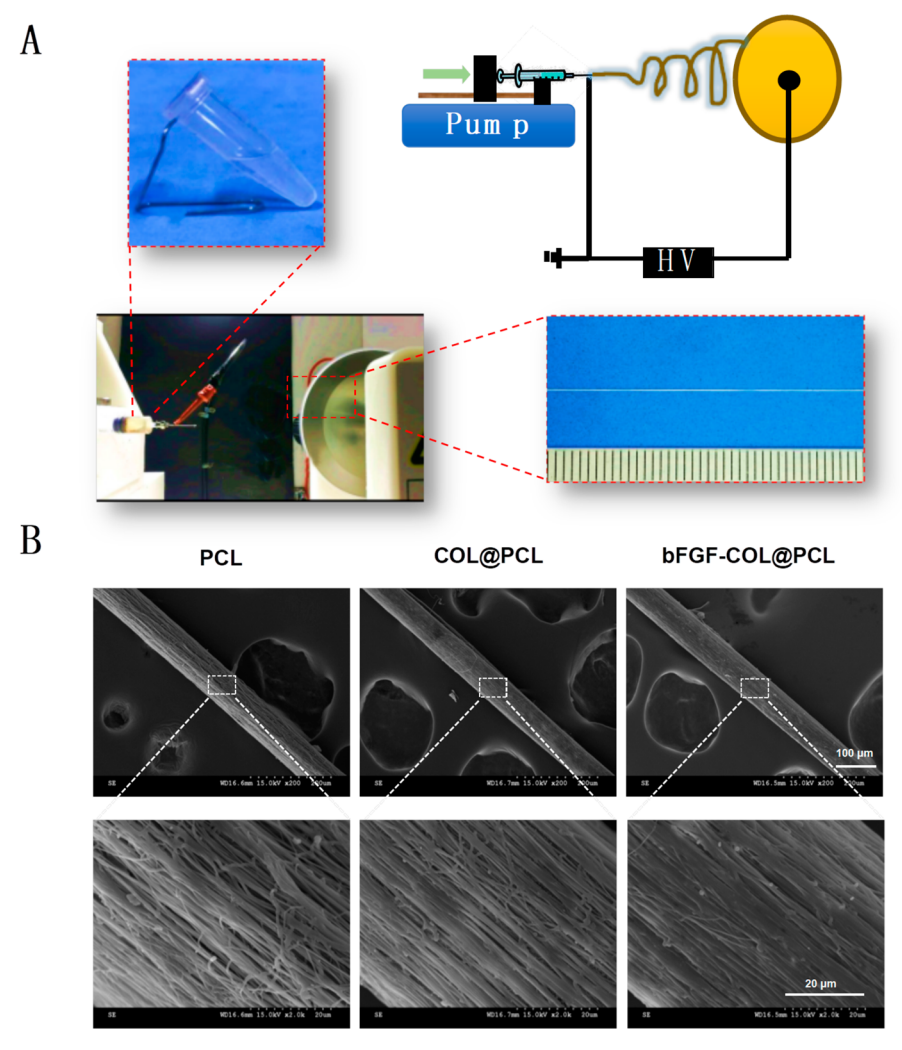


Figure 1. (A) Schematic of a general preparation of PCL-based yarns using an in-house electrospinning. (B) SEM images of PCL, COL@PCL, and bFGF-COL@PCL monofilament at different magnifications of 200× (upper panel) and 2000× (bottom panel).

water for 5 min. Sections were immersed in alcohol with rising concentrations of 80%, 95%, and 100% alcohol for 5 min, respectively, and in xylene for 30 min. Finally, images of stained sections were captured using a Nikon microscope (Nikon, Tokyo, Japan) after covering the tissues by neutral resin and coverslips.

2.9. Masson Trichrome Staining. Sections were deparaffinized and rehydrated as described above, then stained with Masson's trichrome staining kit under the guide of the protocols. 11 Briefly, the sections were stained with A1:A2 (1:1) for 5 min, thoroughly rinsed with water, and covered in acid alcohol for 3 s for differentiation. Staining fibrous tissue was performed for 5 min with ponceau acid fuchsin solution, then stained with 0.2% acetic acid solution for 1 min. Sections were washed and stained with phosphomolybdic acid solution for 30 s for differentiation. Then, tissue was stained with aniline blue for 20 s. The samples were dehydrated and sealed with a glass coverslip. Stained samples were observed, and photographs were obtained by a Nikon microscope (Nikon, Tokyo, Japan).

2.10. AB-PAS Staining. The samples were dewaxed and rehydrated as previously described above and stained with Alcian Blue for 15 min in the dark and then soaked in distilled water for 3 min twice. The tissue was then oxidized with oxidant for 15 min in the dark, immersed in Schiff reagent for 15 min, and then rinsed with running water for 10 min after washing the tissue. Next, after 5 min of stain, excess solutions were removed by rinsing with PBS for 3 min. The samples were dehydrated and sealed with a glass coverslip. Stained samples were photographed using a Nikon microscope (Nikon, Tokyo, Japan).

2.11. Immunohistochemical Staining. Sections were deparaffinized, rehydrated, and covered with 3% H₂O₂ for 15 min which interdicted endogenous peroxidase activity. Then, the skin sections were treated three times with PBS for 5 min each time. The sections were subjected to high-pressure antigen retrieval in sodium citrate buffer and then immersed in 5% BSA for 30 min to block nonspecific antigens. After that, tissues were incubated with primary antibody rabbit antiwide spectrum cytokeratin (1:250) diluted in 1% BSA overnight at 4 °C. Subsequently, after rinsing with PBS, the secondary antibody such as goat antirabbit lgG (H & L) HRP conjugated (1:1000) diluted in PBS was added and further incubated at 37 °C for 1 h. Sections were covered with neutral resin and coverslips. Stained samples were photographed by a Nikon ECLIPSE 80i (Nikon, Tokyo, Japan).

2.12. Immunofluorescent Staining. Sections were treated as immunohistochemistry staining mentioned above until primary antibody is incubated. Skin sections were stained with rabbit polyclonal antibody to CD31 (1:20) and rabbit polyclonal antibody to Ki67 (1:300) diluted in 1% BSA. Next, the samples with goat antirabbit IgG Alexa Fluor 488 (1:1000) and goat antirabbit IgG Alexa Fluor647 (1:1000) diluted in PBS. Whereafter, samples were covered with antifluorescent quenching agent containing DAPI and coverslips. Fluorescent images were captured using a Nikon confocal laser microscope (Nikon, A1 PLUS, Tokyo, Japan).

2.13. Statistical Analysis. All data were analyzed using GraphPad Prism statistical software (GraphPad Software Inc., La Jolla, CA) and represented by mean ± standard deviation. Statistical differences **ACS Applied Bio Materials**

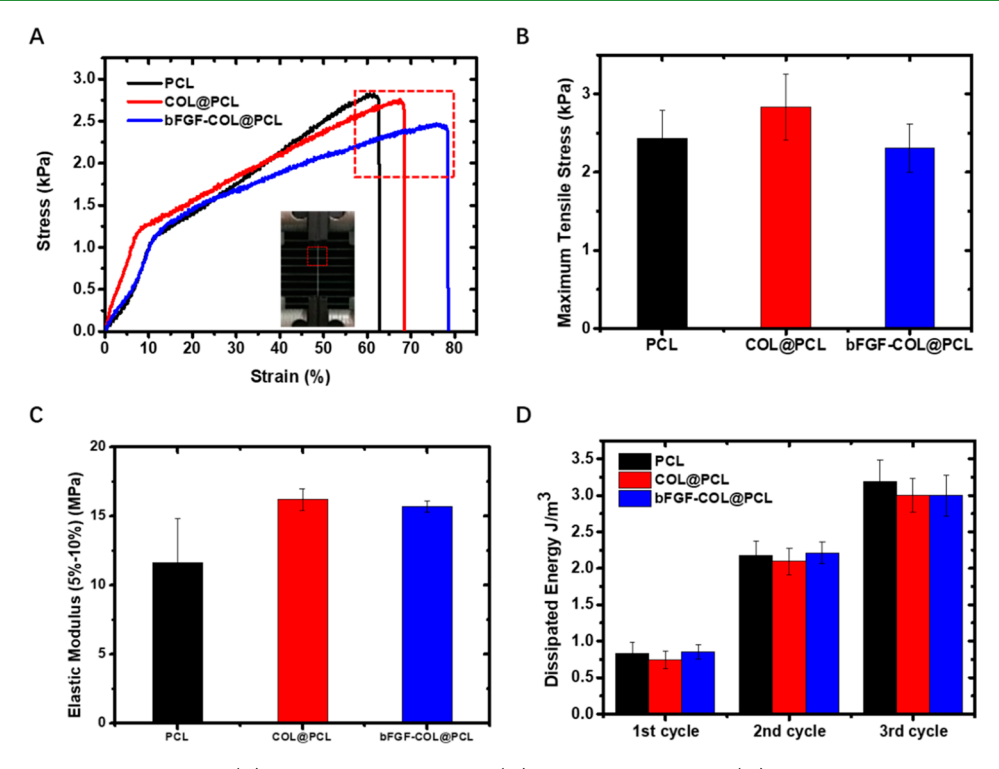


Figure 2. (A) Tensile stress—strain curves, (B) maximum tensile stress, (C) elastic modulus, and (D) dissipated energy of PCL, COL@PCL, and bFGF-COL@PCL sutures.

between different experimental groups were performed by one-way analysis of variance. For all tests, *p value <0.05, **p value <0.01, ***p value <0.001.

3. RESULTS AND DISCUSSION

3.1. Fabrication and Characterization of bFGF-COL@ PCL Sutures. Figure 1A shows an electrospinning process for preparing bFGF-COL@PCL sutures using an in-house rotating edge-sharpened disc collector. By adjusting different electrospinning parameters (e.g., flow rate, applied voltage, distance from needle to collector, and collector rotate speed), we can obtain uniform bFGF-COL@PCL sutures with continuously aligned nanofiber yarns and achieve desirable mechanical properties. We also prepared PCL and COL@PCL sutures for comparison. Typical scanning electron microscopy images in Figure 1B clearly showed that all of three electrospun PCL, COL@PCL, and bFGF-COL@PCL sutures contained well-aligned nanofiber bundles with very smooth nanosized fiber surfaces. The diameters of PCL, COL@PCL, and bFGF-COL@PCL sutures were around 0.1 mm. A closer microscale visual inspection further showed that all three sutures displayed highly aligned fibrous bundles to form yarns with uniform smooth surface, resulting in high drug-loading surface area. No significant differences in morphology and diameter of nanofiber bundles among the three sutures were observed, indicating the encapsulation of collagen and bFGF into the bFGF-COL@PCL sutures would not change the physical morphology of electrospun fiber yarns. In addition, the diameter of nanofibers in these sutures can be easily adjusted by spinning time during the electrospinning process.

Since surgical sutures generally requires strong mechanical properties to close up the separated wound sites, herein synthetic polymer nanofibers (e.g., PCL nanofibers) instead of naturally derived protein nanofibers (e.g., collagen nanofibers) were used to produce electrospun bioscaffolds because of their

excellent mechanical properties (e.g., high tensile strength and distinct viscoelastic and rheological properties). To better assess the impact of the loading of collagen and bFGF on mechanical properties of PCL fibrous sutures, we conducted tensile tests to determine and compare the mechanical properties between three PCL, COL@PCL, and bFGF-COL@PCL sutures. Figure 2A-C showed that PCL, COL@ PCL, and bFGF-COL@PCL sutures achieved a maximum tensile strength/elastic moduli of 2.43 \pm 0.30 kPa/11.62 \pm 0.26 kPa at 63% strain, 2.83 \pm 0.34 kPa/16.20 \pm 0.67 kPa at 68% strain, and 2.31 \pm 0.25 kPa/15.71 \pm 0.33 at 78% strain, respectively. Different from conventional multifilament-braided sutures, our electrospinning sutures are made of monofilaments with much smoother morphology. If our sutures are made of multifilaments, their mechanical strength can be greatly improved. On the other hand, we should note that since the skin of mouse is very soft and elastic, it is more important to use sutures with similar soft-elastic properties to skin properties. We found that more rigid and tough sutures often lead to wounds that are difficult for healing. Our sutures with 3 kPa of tensile strength and 10 MPa of elastic modulus can best achieve the fast wound healing process without breakage. It appears that the loading of COL and bFGF into PCL fibers slightly increased tensile stress, strain, and elastic moduli, suggesting the enhanced mechanical property by the addition of COL and bFGF. Further statistical analysis showed that (i) mechanical retention is mainly attributed to highly aligned nanofilament bundles in the three PCL-based sutures and (ii) the loading of bFGF and COL does not significantly alter the packing and alignment of PCL nanofilaments (Figure

Further cyclic loading—unloading tensile testing was carried out to examine the energy dissipation capacity of the three PCL-based sutures (Figure S1). Upon deriving the data from stress—strain curves from Figure S1, Figure 2D displays and

compares the energy dissipation of each loading-unloading cycle for the three PCL-based sutures as tensile strain increased from 20% to 60%. It can be seen that for each cycle all three sutures exhibited similar hysteresis loops, indicating that the loading of COL or bFGF into PCL nanofibers to form a hybrid structure does not induce any significant change in energy dissipation, consistent with tensile stress-strain data. Meanwhile, all three PCL-based sutures showed the almost same trend of the increase of hysteresis loops as strains, i.e., dissipated energy of the three sutures increased from 0.81 J/m³ at the first cycle to 2.16 J/m³ at the second cycle, and to 3.06 J/m³ at the third cycle. This indicates that the PCL-based sutures undergo partial self-recovery during the unloading process. Taken together, the PCLbased sutures have similar energy dissipation and toughening mechanisms, mainly because they adopt similar fibrous structures of well-aligned bundles.

3.2. Loading and Release of bFGF from bFGF-COL@ PCL Sutures. Upon electrospinning, bFGF was infiltrated into COL@PCL nanofiber yarns. Using fluorescence dye of Cy5 to label bFGF, Figure 3A confirmed that the successful loading

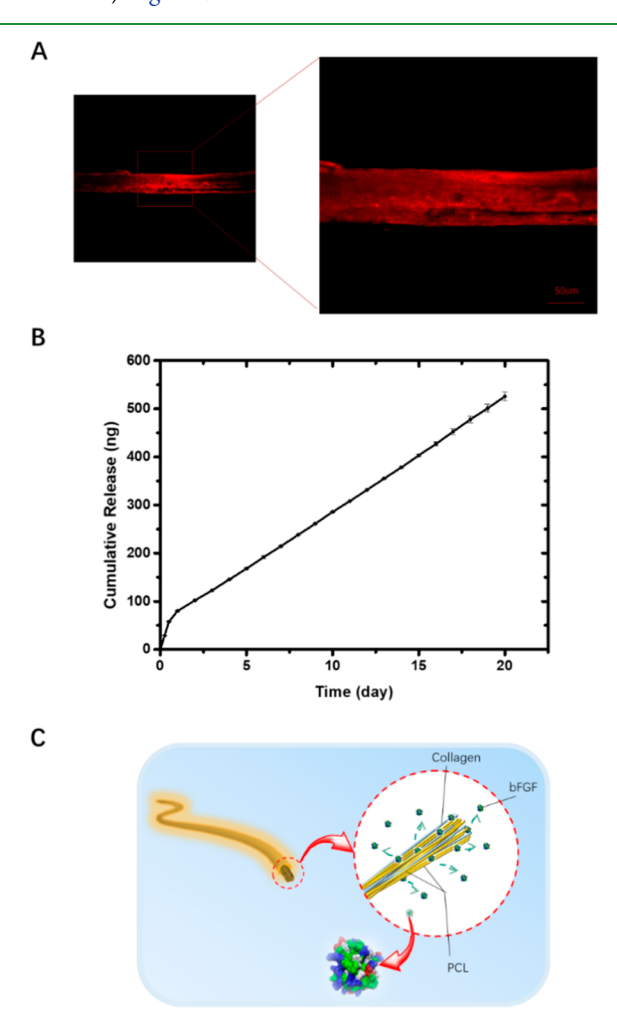


Figure 3. (A) bFGF-COL@PCL sutures with cy5-labled bFGF as indicated by confocal fluorescence. (B) *In vitro* release kinetics of bFGF from bFGF-COL@PCL sutures in PBS buffer by ELISA. (C) Schematic of a two-step release mechanism of bFGF from three-dimensional COL/PCL structures, starting with initial fast release of bFGF from suture surface, followed by the diffusion-degradable-controlled slow release bFGF from suture interior.

and distribution of bFGF at both outside and inside the PCL aligned nanofiber yarns. The bFGF loading ratio was calculated to be ~0.3 wt %. Further, the release of bFGF from bFGF-COL@PCL sutures was studied in saline at room temperature using the ELISA assay over 21 days. As shown in Figure 3B,C, bFGF release behavior showed a typical two-phase releasing kinetics, i.e., an initial burst release within the first 24 h at a release rate of 4.3 ng/h, followed by a slow and gradual constant release at 2.1 ng/h between day 2 and day 21. The final release percentage of bFGF from bFGF-COL@PCL sutures was estimated to be 31.6 wt %. Such bFGF release profile suggests a location-controlled release behavior, i.e., bFGF located on the surface of bFGF-COL@PCL fibers experienced a rapid release at the initial burst-release stage, while bFGF buried inside of bFGF-COL@PCL fibers had difficulty being released because of a high diffusion barrier and slow suture degradation, both of which restrict the release of bFGF from bFGF-COL@PCL nanofiber bundles at the second stage. Figure S4 show the degradation time of the sutures using in vivo results. As a control, Vicryl sutures on wounds degraded very fast and completely disappeared on day 3. Differently, pure PCL sutures started to break down on day 5, while both bFGF-COL@PCL and COL@PCL sutures experienced the even slower degradation and gradually disappeared in accompanied by the wound healing process. Meanwhile, the release of bFGF from and the presence of collagen in bFGF-COL@PCL sutures can still remain their bioactivity to synergistically promote wound regeneration, resulting in the better healing efficiency than commercialized degradable Vicryl suture. Overall, this sequential and biphasic release of bFGF from nanofiber surfaces to inner nanofibers in bFGF-COL@PCL sutures further demonstrate the successful loading of bFGF into electrospun nanofibers for achieving a sustainable release of loaded bFGF.

3.3. bFGF-COL@PCL Enhances in Vivo Wound Healing. Upon demonstrating mechanical properties and sustainable bFGF release of bFGF-COL@PCL sutures, we further applied both COL@PCL and bFGF-COL@PCL sutures to an incision wound model in vivo and sew the wounds with both sutures, in comparison with pure PCL suture and Vicryl (as a commercial suture) as controls. Figure 4A shows the sequential images of the stitched wounds in mice treated with four different surgical sutures during 13 postoperative days, while Figure 4B,C shows the dermoscopic images and traces of wound beds on day 5 and day 13 at the greater details of the wound bed. As shown in Figure 4A, compared to pure PCL suture-treated wound, COL@PCL and bFGF-COL@PCL accelerated wound closure at almost all time points with enhanced wound healing behavior, and no obvious sign of infection or inflammation was observed at the wound area, indicating that both collagen and bFGF promote wound remolding. Particularly, at day 13, the wounds stitched by bFGF-COL@PCL sutures was completely healed and almost scarless, while other suture-treated wounds still retained some observable unhealed wound areas without inflammation and exudate. Figure 4B further shows dermoscopic images of the four sutured treated wounds at day 5 and day 13. On day 5, except the PCL suture-treated wound, all of the other wounds treated by Vicryl, COL@PCL, and bFGF-COL@PCL were well connected and sealed by the sutures. Obviously, bFGF-COL@PCL-treated wound was almost healed by ~50% as compared to other wounds. The trace of wounds in Figure 4B also confirmed that different from the bFGF-COL@PCL-

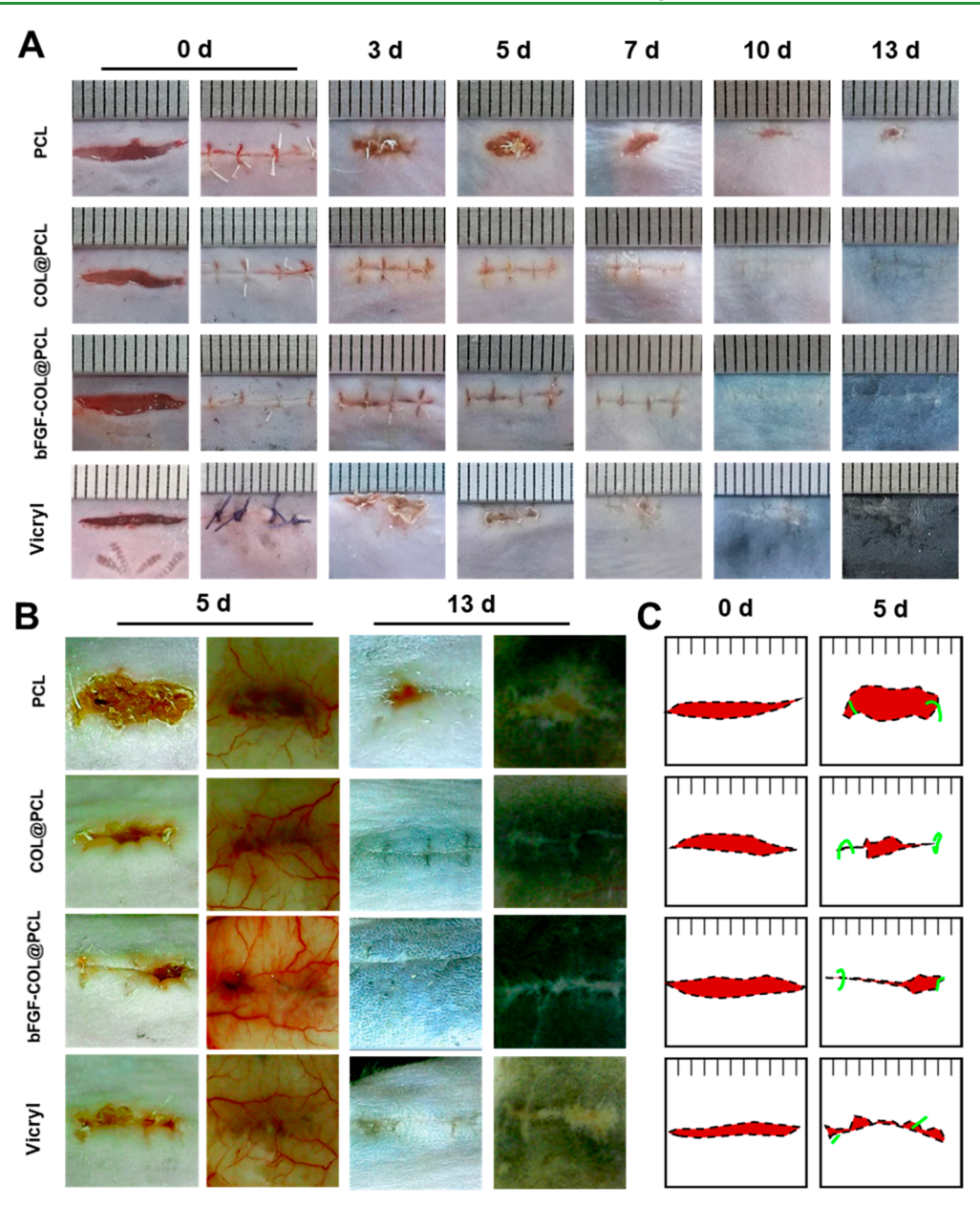


Figure 4. In vitro wound healing efficacy of the four PCL, COL@PCL, bFGF-COL@PCL, and Vicryl sutures. (A) Representative images of time-evolved wound closure treated with PCL, COL@PCL, bFGF-COL@PCL, and Vicryl sutures at different time points of 0, 3, 5, 7, 10, and 13 days. (B) Detailed dermoscopic images of the outside and inside wounds treated with PCL, COL@PCL, bFGF-COL@PCL, and Vicryl sutures on days 5 and 13. (C) Wound closure trace of PCL, COL@PCL, bFGF-COL@PCL, and Vicryl sutures on days 0 and 5.

treated wound, tissue defects in the other suture-treated wounds were still observed in the dermis. This phenomenon became even more pronounced on day 13. After 13 days, as compared to the other three wounds with red and uneven scars, the wound treated with bFGF-COL@PCL sutures was completely closed and the wound morphology was close to the normal skin, indicating that the presence and release of both bFGF and collagen indeed accelerate the wound healing. These suture-treated wound healing results indicate that the release of bFGF and the presence of collagen in bFGF-COL@PCL sutures remain their bioactivity and thus synergistically promote wound regeneration, even better than the commercialized Vicryl suture. 30

3.4. bFGF-COL@PCL Suture Promotes Granulation Tissue Formation, Collagen Deposition, and Re-Epithelization *in Vivo*. To further examine the effect of bFGF-

COL@PCL on different healing aspects (i.e., granulation tissue formation, collagen deposition, and re-epithelization) of incision wound sites, ³¹ the four suture-treated wounds were H&E stained in Figure 5 on days 5 and 13. On day 5, H&E stained images showed that the wounds treated with Vicryl, PCL, and COL@PCL sutures still remained some unhealed regions as evidenced by the thin and transparent damaged skins. Differently, bFGF-COL@PCL sutures promoted the earlier granulation tissue formation with dense collagen deposition. On day 13, all of the PCL-derived nanofibrous sutures completely closed the wounds with some new neo-epidermis formation. Side-by-side comparison of H&E stained wounds still revealed that skin appendage and hair follicles in bFGF-COL@PCL group were much higher than the other three groups.

ACS Applied Bio Materials www.acsabm.org Article

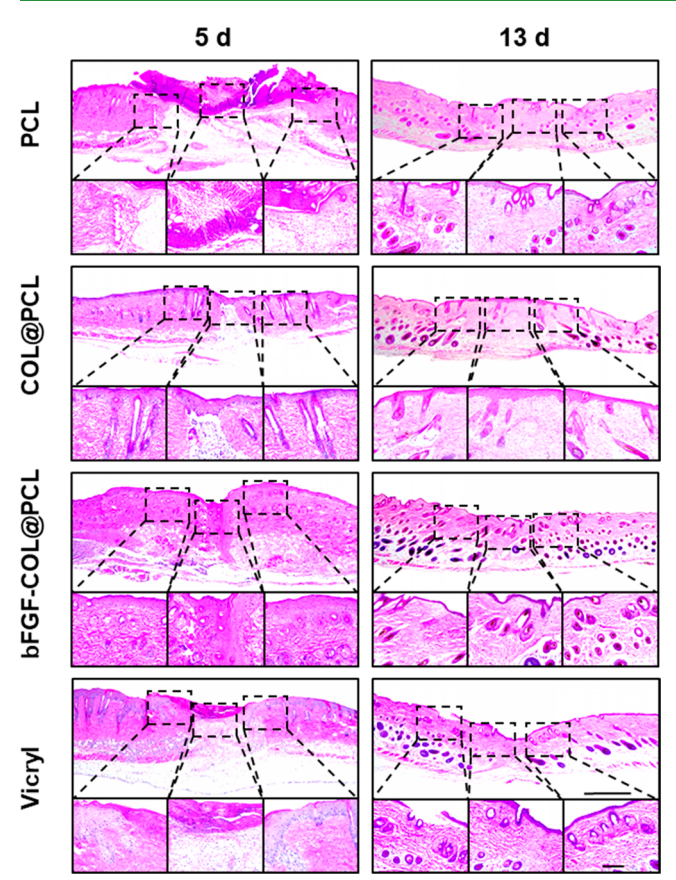


Figure 5. Representative hematoxylin and eosin (H&E)-stained images for skin wounds treated with PCL, COL@PCL, bFGF-COL@PCL, and Vicryl sutures on days 5 and 13 (original scale bar = 500 μ m). Dashed box presents the corresponding higher magnification H&E of wound bed centers and edge (close-up scale bar = 100 μ m).

H&E stained results were also confirmed by MT staining (collagens were stained in blue, while keratins and muscle fibers were stained in pink) as shown in Figure 6A of the wounds on day 5 and day 13 to demonstrate the collagen regenerated in the treated wounds. It can be seen that bFGF-COL@PCL-treated wounds showed the densest collagen deposition, as compared to the other three suture-treated wounds with deficient collagen expression. Moreover, the collagen fibers in the bFGF-COL@PCL group were well organized with intact skin appendage structure, which is morphologically similar to normal skin. Quantitatively, Figure 6B,C shows the statistical analysis of collagen deposition on days 5 and 13. Clearly, the mean collagen deposition density on day 5/day 13 was 5.5/6.6 for PCL, 6.7/8.6 for COL@PCL, 11.4/12.0 for bFGF-COL@PCL, and 7.1/7.9 for Vicryl, respectively. Clearly, the bFGF-COL@PCL-treated wounds represented almost a 2-fold increase in collagen deposition, as compared to the other three wounds treated with PCL, COL@ PCL, and Vicryl. Such accelerated granulation tissue formation and collagen deposition became even more pronounced on day 13. Thus, both H&E and MT stained results indicate that the sustainable release of bFGF growth factors and the presence of collagens in the PCL sutures can synergistically promote the earlier granulation tissue formation and the more dense collagen deposition due to the bFGF-stimulated cell proliferation, differentiation, and migration. 32,33

During the wound healing process, re-epithelialization of the damaged skin is equally important to granulation tissue formation and collagen deposition. Immunohistochemical staining of cytokeratin was used to evaluate re-epithelialization in wounds treated with different sutures on day 5 and day 13. As shown in Figure 7A, both COL@PCL and bFGF-COL@ PCL groups and both COL@PCL and bFGF-COL@PCL groups exhibit the faster re-epithelization than pure PCL and commercialized Vicryl groups, as evidenced by the facts that both COL@PCL and bFGF-COL@PCL groups facilitated the earlier epithelization without any observable scab by expressing more keratinocytes and forming the thicker epidermis. In parallel, we quantitatively analyzed the unhealed epithelium for the four suture groups, showing a decreased order of unregenerate wounds: PCL (2.9 mm) > Vicryl (1.5 mm) > COL@PCL (0.22 mm) > bFGF-COL@PCL (0.17 mm) (Figure 7B). Further quantification of the regenerated thickness of the epithelium was collected in Figure 7C, where the thickness of the newly covered epidermis was 117.18 \pm 33.39 μ m for PCL, 98.09 \pm 21.06 μ m for COL@PCL, $655.85 \pm 60.87 \,\mu\text{m}$ for bFGF-COL@PCL, and 173.27 ± 38.97 µm for Vicryl groups, respectively. After 13 days of wound healing, more and denser hair follicles beneath the healed epidermis were observed in the dermal layer of the incision site of the bFGF-COL@PCL group, in sharp contrast to the PCL, COL@PCL, and Vicryl groups. All these results confirm that the bFGF-COL@PCL suture can greatly accelerate the regeneration of neo-epidermis and hair follicles, demonstrating the faster wound healing effect of released bFGF on the reepithelization of wounds in vivo.

3.5. bFGF-COL@PCL Suture Improves the Basement Membrane (BM) Reconstruction. A suture is a medical device used to hold wound tissues tightly and safely together. After the closing-up of the incision of wounds by external forces, basement membrane (BM) is used to connect the epithelium and its underneath dermal layer starts to play an indispensable role in wound remolding and skin regeneration.³⁴ BM constituted as an extracellular microenvironment sensor or regulator for both epithelial cells and dermal cells.³⁵ Previous reports have shown that fibroblast growth factors (FGFs) could alter the adhesiveness, proliferation, as well as migration behavior of epithelial cells from BM, thereby regulating more epithelia cell-surface anchors (e.g integrin) from the surrounding extracellular matrix.³⁶ Herein, the delivery of bFGF to wound sites support the positive migration of epithelial cells, confirming the enhanced healing efficiency of our bFGF-COL@PCL suture. Figure 8 presents the Periodic Acid-Schiff (PAS) staining of the BM of all four suture groups on day 5 to examine the reconstruction of the BM. A close-up visual inspection of three specific wound sites (i.e., left edge, middle center, and right edge) showed that all of the four suture groups attained homogeneous PAS cell staining at both the left and right edges of the wounds with no significant differences, suggesting wound repairing first occurs at the edge regions. However, the four suture groups displayed different PAS staining at the middle center region of wounds. As a control, micrographs of the central wound area in mice treated with PCL suture showed a large reduction of PAS deposition and severely impairs with irregular patchy distribution. Both Vicryl and COL@PCL groups presented the better integrity and morphology of BM but still with residual hiatus between the epithelium and dermis, indicating the partial BM reconstruction. In a sharp contrast, bFGF-COL@PCL suture

ACS Applied Bio Materials

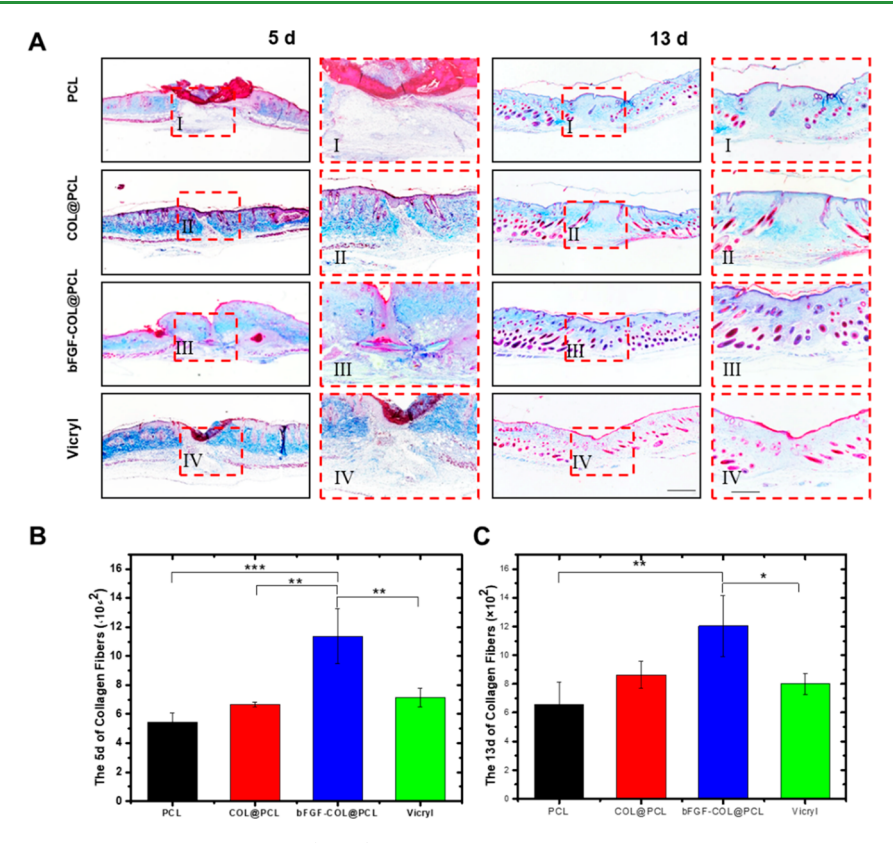


Figure 6. (A) Histological Masson's trichrome-staining (MTS) revealed collagen deposition upon wound site treated with PCL, COL@PCL, bFGF-COL@PCL, and Vicryl sutures on days 5 and 13 (original scale bar = $500 \, \mu \text{m}$). Dashed box presents the corresponding higher magnification MTS images of wound bed centers (close-up scale bar = $100 \, \mu \text{m}$). (B) Quantified expression of collagen fibers density on day 5. (C) Quantified expression of collagen fibers density on day 13 for PCL, COL@PCL, bFGF-COL@PCL, and Vicryl sutures. Statistical differences were performed using ANOVA. ***P < 0.001, **P < 0.01, **P < 0.05, *n > 3.

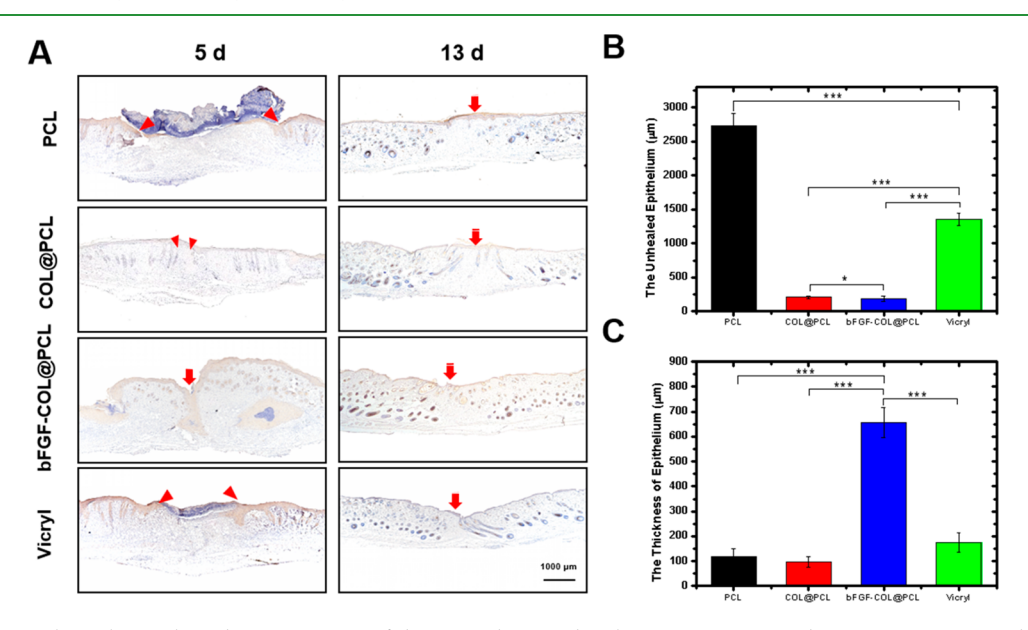


Figure 7. (A) Immunohistochemical cytokeratin staining of skin wounds treated with PCL, COL@PCL, bFGF-COL@PCL, and Vicryl sutures on days 5 and 13. (B) Quantified unhealed epithelium and (C) epithelium thickness of skin wounds treated with PCL, COL@PCL, bFGF-COL@PCL, and Vicryl sutures on day 5. Scale bar = 1000 μ m, Significant difference between samples is defined by ***P < 0.001, **P < 0.05, n > 5.

facilitated a fully regeneration at both edges and the center of the wound areas, which tightly jointed the epithelium to its underneath dermals to reproduce almost intact BM. These data confirmed that the sustained release of bFGF promotes the recruitment of endothelial cells to the wound area and enhances the reconstruction of BM.

3.6. bFGF-COL@PCL Suture Accelerates Cell Proliferation and Angiogenesis. Ki67, as a typical biomarker of the cell cycle, is often used to quantify cell proliferation at the

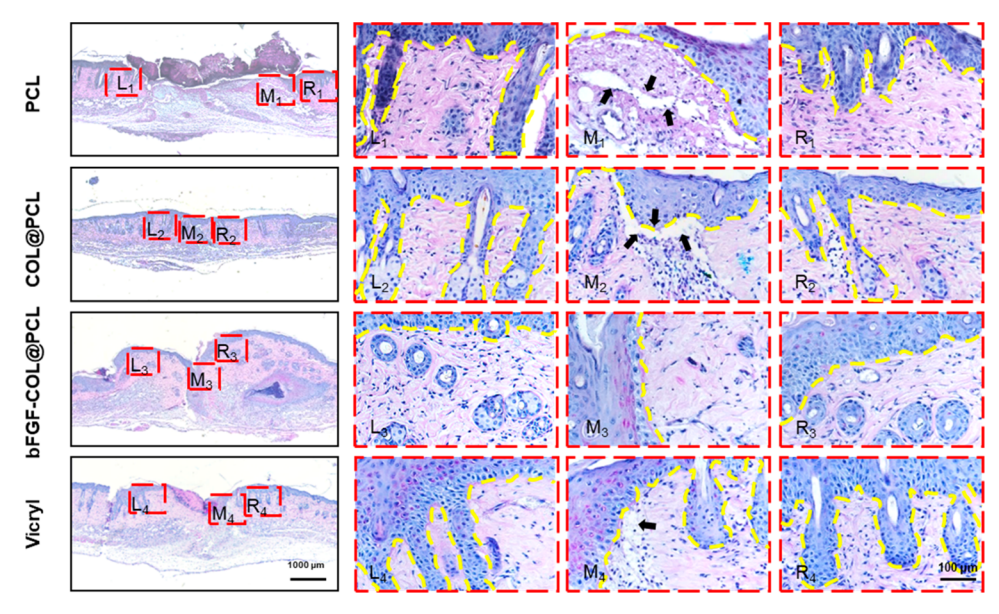


Figure 8. AB-PAS staining of the basement membrane (BM) of skin wounds treated with PCL, COL@PCL, bFGF-COL@PCL, and Vicryl sutures on day 5 (original scale bar = $1000 \ \mu m$). L_x , M_x , and R_x (x = 1, 2, 3, 4) represents the higher magnification images of wound beds at the left, middle, and right regions for each suture group, respectively (close-up scale bar = $100 \ \mu m$).

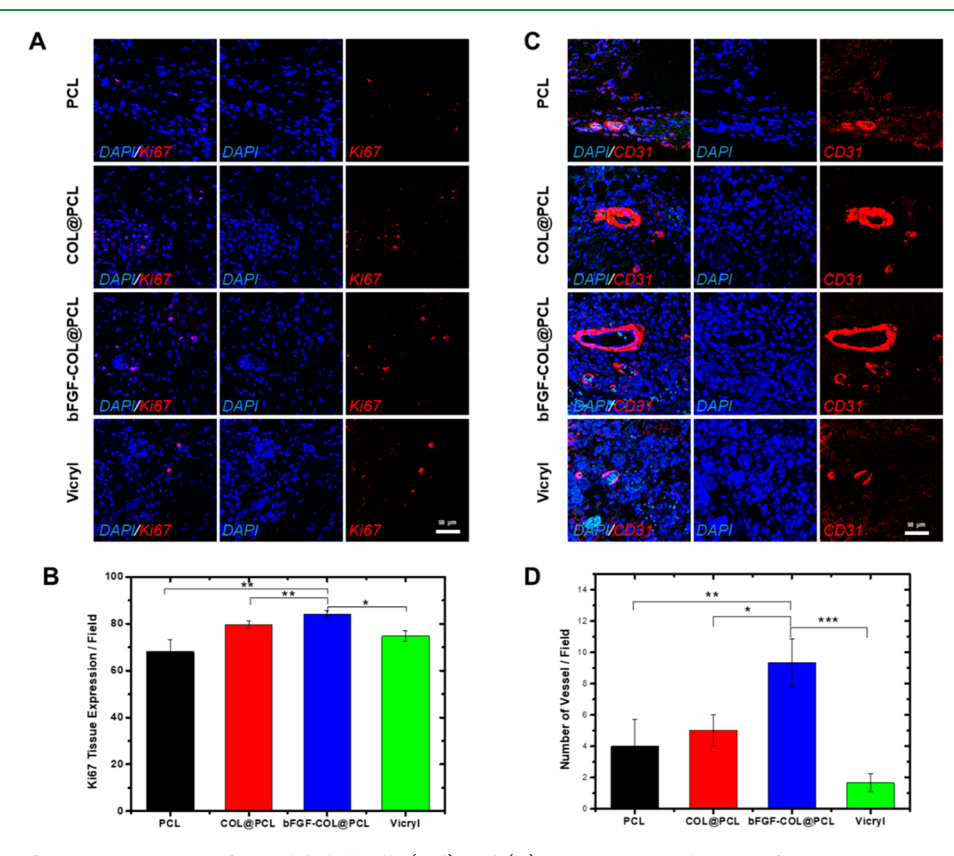


Figure 9. (A) Immunofluorescent staining of Ki67-labeled cells (red) and (B) quantitative evaluation of Ki67 expression on wounds treated with PCL, COL@PCL, bFGF-COL@PCL, and Vicryl sutures on day 5 (scale bar = $50 \mu m$). (C) Immunofluorescent staining of vascular endothelial cells marker CD31 (red) and (D) quantitative evaluation of blood vessel numbers by CD31 on wounds treated with PCL, COL@PCL, bFGF-COL@PCL, and Vicryl sutures on day 5. Significant difference between samples is defined by ***P < 0.001, **P < 0.01, **P < 0.05, *P < 0

mitotic phase.³⁷ Here, immunofluorescent staining of Ki67 was performed to determine the proliferation state of the cells at the wound site. Figure 9A showed that upon the incision wound on day 5, both the PCL and COL@PCL suture groups exhibited a low density of Ki67 expression, indicating low levels of cell proliferation. In contrast, incision wound treated

with bFGF-COL@PCL and Vicryl sutures illustrated the most significant enhancement (p < 0.05) in cell proliferation. Statistical analysis in Figure 9B showed that bFGF-COL@PCL suture (83.96 \pm 1.66%) induced the higher expression density of Ki67 than PCL (68.12 \pm 5.27%), COL@PCL (79.55 \pm 1.63%), and Vicryl (74.80 \pm 2.31%) sutures.

Angiogenesis is also another important factor for good wound repair. Further neovascularization was quantitatively evaluated by CD 31 (vascular endothelial cells marker) labeling, representing newly formed blood vessels during healing in wound bed on day 5. As shown in Figure 9C, bFGF-COL@PCL suture significantly increased the formation of new blood capillaries in the granulation tissues on the wound center and dermal edge with the largest lumen area. Further comparison of the expressions of CD 31 in Figure 9D revealed a decreased order for the formation of vessels per field between all four suture groups, i.e., bFGF-COL@PCL (9.33 \pm 1.5) > COL@PCL (5.00 + 1.00) > PCL (4.00 + 1.73) > Vicrylgroup (1.67 ± 0.58). Interestingly, all of the PCL-based sutures demonstrated major enhancement in cell proliferation and angiogenesis as compared to the commercial Vicryl suture. particularly bFGF-loaded sutures produced 5-fold higher angiogenesis than the commercialized Vicryl suture. Taken together, the addition and sustained release of bFGF from PCL nanofibers indeed enhanced cell proliferation and thus induced better neovascularization.^{38,39}

Furthermore, previous studies indicated that macrophage polarization is very important for wound regeneration. ^{39–41} We further quantified and compared the M1 and M2 macrophages of the in-house made sutures (PCL, COL@ PCL and bFGF-COL@PCL) as compared to the Vicryl control group. It can be seen in Figure S3 that the M2/M1 percentage in the bFGF-COL@PCL group was much higher than that in other groups, indicating that up-regulation of M2 macrophage polarization leads to the enhanced wound regeneration. In line with wound closure rate data, macrophage polarization results again confirm the positive role of bFGF-COL@PCL in wound regeneration.

4. CONCLUSIONS

In this work, we fabricated electrospun bFGF-COL@PCL surgical sutures by incorporating both collagen and bFGF into biodegradable PCL fibrous matrix. First, the resultant bFGF-COL@PCL surgical sutures adopted highly aligned nanofibers, which offered high surface area to improve mechanical properties, increase loading efficiency of bFGF up to 33.3%, and achieve sustainable control-release of bFGF up to 21 days. Then, bFGF-COL@PCL surgical sutures were applied to in vivo incision acute wounds in mice. Collective wound healing results demonstrated that bFGF-COL@PCL sutures exhibited the better wound healing efficiency in vivo than PCL, COL@ PCL, and Vicryl sutures, as evidenced by enhanced granulation formation, collagen deposition, and re-epithelialization. The presence of both collagen and bFGF in PCL sutures synergistically promoted BM construction, cell proliferation, and angiogenesis at the early stage of wound repairs. This work offers a new yet simple strategy to develop biocompatible and effective surgical sutures for regenerative tissue engineering. Finally, we added our personal remarks on the future development of surgical sutures. From materials design and suture function viewpoints, suture materials made of natural proteins (e.g., collagen, gelatin, silk) or synthetic polymers (e.g., polysaccharides, polyurethanes, PEGs) need to be integrated with more and smarter functions (e.g., stimuliresponsive, biofouling, biodegradable, bioinsiration) and bioactive drugs and molecules (e.g., growth factors, antibacterial drugs, antithrombotic drugs, antiscarring drugs, anesthetic agents) for better management of pathological scarring and wound healing. From the fabrication viewpoint,

different technologies (e.g., electrospinning, radical polymerization) need to be developed to fabricate advanced scaffolds with different structures (e.g., core—shell fibrous scaffolds, multilayer scaffolds, and surface modified scaffolds) and desirable mechanical properties.

ASSOCIATED CONTENT

Supporting Information

The Supporting Information is available free of charge at https://pubs.acs.org/doi/10.1021/acsabm.9b01000.

Tensile properties of PCL, COL@PCL, and bFGF-COL@PCL sutures; mouse weight loss treated with different sutures; M2 and M1 expression on *in vivo* wounds treated with different sutures; and degradation of different sutures on *in vivo* wounds (PDF)

AUTHOR INFORMATION

Corresponding Authors

Huacheng He — College of Chemistry and Materials Engineering, Wenzhou University, Wenzhou 325027, P.R. China; Email: heh@wu.edu.cn

Jie Zheng — Department of Chemical and Biomolecular Engineering, The University of Akron, Akron, Ohio 44325, United States; © orcid.org/0000-0003-1547-3612; Email: zhengj@uakron.edu

Jiang Wu − School of Pharmaceutical Sciences, Key Laboratory of Biotechnology and Pharmaceutical Engineering, Wenzhou Medical University, Wenzhou 325035, P.R. China; orcid.org/0000-0003-1929-3328; Email: woody870402@hotmail.com

Authors

Jinyu Hu — School of Pharmaceutical Sciences, Key Laboratory of Biotechnology and Pharmaceutical Engineering, Wenzhou Medical University, Wenzhou 325035, P.R. China

Yi Song — School of Pharmaceutical Sciences, Key Laboratory of Biotechnology and Pharmaceutical Engineering, Wenzhou Medical University, Wenzhou 325035, P.R. China

Cuiyun Zhang — School of Pharmaceutical Sciences, Key Laboratory of Biotechnology and Pharmaceutical Engineering, Wenzhou Medical University, Wenzhou 325035, P.R. China

Wen Huang – School of Pharmaceutical Sciences, Key Laboratory of Biotechnology and Pharmaceutical Engineering, Wenzhou Medical University, Wenzhou 325035, P.R. China

Anqi Chen — School of Pharmaceutical Sciences, Key Laboratory of Biotechnology and Pharmaceutical Engineering, Wenzhou Medical University, Wenzhou 325035, P.R. China

Susu Zhang — School of Pharmaceutical Sciences, Key Laboratory of Biotechnology and Pharmaceutical Engineering, Wenzhou Medical University, Wenzhou 325035, P.R. China

Yanxin Chen — College of Chemistry and Materials Engineering, Wenzhou University, Wenzhou 325027, P.R. China

Chaodong Tu — School of Pharmaceutical Sciences, Key Laboratory of Biotechnology and Pharmaceutical Engineering, Wenzhou Medical University, Wenzhou 325035, P.R. China

Jianhui Liu – School of Pharmaceutical Sciences, Key Laboratory of Biotechnology and Pharmaceutical Engineering, Wenzhou Medical University, Wenzhou 325035, P.R. China

Xuan Xuan – School of Pharmaceutical Sciences, Key Laboratory of Biotechnology and Pharmaceutical Engineering, Wenzhou Medical University, Wenzhou 325035, P.R. China; The First Affiliated Hospital of Wenzhou Medical University, , Wenzhou 325000, P. R. China

Yung Chang — R&D Center for Membrane Technology and Department of Chemical Engineering, Chung Yuan Christian University, Chung-Li 320, Taiwan; ⊙ orcid.org/0000-0003-1419-4478

Complete contact information is available at: https://pubs.acs.org/10.1021/acsabm.9b01000

Author Contributions

*J.H. and Y.S. contributed equally to this work.

Notes

The authors declare no competing financial interest.

ACKNOWLEDGMENTS

H.H. thanks the financial support from Zhejiang Provincial Natural Science Foundation of China (Grant LGF19H180008), National Natural Science Funding of China (Grant 81701809), Zhejiang Qianjiang Talent Project (Grant QJD1803015). J.W. thanks the financial support from National Natural Science Funding of China (Grant 81601615). J.Z. thanks the financial support from Grant NSF-1806138.

REFERENCES

- (1) Nemoto, M.; Kumazawa, K.; Uchinuma, E.; Kounoike, N.; Takeda, A. Clinical Features of Primary Vein Grafts in Free Tissue Transfers. *Plastic Surgery International* **2015**, 2015, 481402.
- (2) Yang, G.; Lin, H.; Rothrauff, B. B.; Yu, S.; Tuan, R. S. Multilayered polycaprolactone/gelatin fiber-hydrogel composite for tendon tissue engineering. *Acta Biomater.* **2016**, *35*, *68*–76.
- (3) Jiang, J.; Wan, W.; Ge, L.; Bu, S.; Zhong, W.; Xing, M. Mussel-inspired nanofibrous sheet for suture-less stomach incision surgery. *Chem. Commun.* **2015**, *51* (41), 8695–8698.
- (4) Bae, S.; Dibalsi, M. J.; Meilinger, N.; Zhang, C.; Beal, E.; Korneva, G.; Brown, R. O.; Kornev, K. G.; Lee, J. S. Heparin-Eluting Electrospun Nanofiber Yarns for Antithrombotic Vascular Sutures. *ACS Appl. Mater. Interfaces* **2018**, *10* (10), 8426–8435.
- (5) Champeau, M.; Thomassin, J.-M.; Tassaing, T.; Jerome, C. Current manufacturing processes of drug-eluting sutures. *Expert Opin. Drug Delivery* **2017**, *14*, 1293.
- (6) Padmakumar, S.; Joseph, J.; Neppalli, M. H.; Mathew, S. E.; Nair, S. V.; Shankarappa, S. A.; Menon, D. Electrospun Polymeric Core—sheath Yarns as Drug Eluting Surgical Sutures. *ACS Appl. Mater. Interfaces* **2016**, 8 (11), 6925–6934.
- (7) Li, J.; Linderman, S. W.; Zhu, C.; Liu, H.; Thomopoulos, S.; Xia, Y. Surgical Sutures with Porous Sheaths for the Sustained Release of Growth Factors. *Adv. Mater.* **2016**, 28 (23), 4620–4624.
- (8) Reckhenrich, A. K.; Kirsch, B. M.; Wahl, E. A.; Schenck, T. L.; Rezaeian, F.; Harder, Y.; Foehr, P.; Machens, H.; Egana, J. T. Surgical Sutures Filled with Adipose-Derived Stem Cells Promote Wound Healing. *PLoS One* **2014**, *9* (3), No. e91169.
- (9) Gu, Z.; Yin, H.; Wang, J.; Ma, L.; Morsi, Y.; Mo, X. Fabrication and characterization of TGF-β1-loaded electrospun poly (lactic-coglycolic acid) core-sheath sutures. *Colloids Surf.*, B **2018**, 161, 331–338.
- (10) Younesi, M.; Donmez, B. O.; Islam, A.; Akkus, O. Heparinized collagen sutures for sustained delivery of PDGF-BB: Delivery profile and effects on tendon-derived cells In-Vitro. *Acta Biomater.* **2016**, *41*, 100–109.
- (11) Wu, J.; Ye, J.; Zhu, J.; Xiao, Z.; He, C.; Shi, H.; Wang, Y.; Lin, C.; Zhang, H.; Zhao, Y.; Fu, X.; Chen, H.; Li, X.; Li, L.; Zheng, J.; Xiao, J. Heparin-based coacervate of FGF2 improves dermal regeneration by asserting a synergistic role with cell proliferation and endogenous facilitated VEGF for cutaneous wound healing. *Biomacromolecules* **2016**, *17* (6), 2168–2177.

- (12) Wu, J.; Zhu, J.; He, C.; Xiao, Z.; Ye, J.; Li, Y.; Chen, A.; Zhang, H.; Li, X.; Lin, L.; Zhao, Y.; Zheng, J.; Xiao, J. Comparative Study of Heparin-Poloxamer Hydrogel Modified bFGF and aFGF for in Vivo Wound Healing Efficiency. ACS Appl. Mater. Interfaces 2016, 8 (29), 18710–18721.
- (13) Guan, D.; Mi, J.; Chen, X.; Wu, Y.; Yao, Y.; Wang, L.; Xiao, Z.; Zhao, Y.; Chen, B.; Dai, J. Lung endothelial cell-targeted peptideguided bFGF promotes the regeneration after radiation induced lung injury. *Biomaterials* **2018**, *184*, 10–19.
- (14) Ono, I.; Akasaka, Y.; Kikuchi, R.; Sakemoto, A.; Kamiya, T.; Yamashita, T.; Jimbow, K. Basic fibroblast growth factor reduces scar formation in acute incisional wounds. *Wound Repair and Regeneration* **2007**, *15* (5), 617–623.
- (15) Shi, H.-X.; Lin, C.; Lin, B.-B.; Wang, Z.-G.; Zhang, H.-Y.; Wu, F.-Z.; Cheng, Y.; Xiang, L.-J.; Guo, D.-J.; Luo, X.; Zhang, G.-Y.; Fu, X.-B.; Bellusci, S.; Li, X.-K.; Xiao, J. The anti-scar effects of basic fibroblast growth factor on the wound repair in vitro and in vivo. *PLoS One* **2013**, *8* (4), No. e59966.
- (16) Sun, X.; Cheng, L.; Zhao, J.; Jin, R.; Sun, B.; Shi, Y.; Zhang, L.; Zhang, Y.; Cui, W. bFGF-grafted electrospun fibrous scaffolds via poly(dopamine) for skin wound healing. *J. Mater. Chem. B* **2014**, 2 (23), 3636–3645.
- (17) Cheng, L.; Sun, X.; Zhao, X.; Wang, L.; Yu, J.; Pan, G.; Li, B.; Yang, H.; Zhang, Y.; Cui, W. Surface biofunctional drug-loaded electrospun fibrous scaffolds for comprehensive repairing hypertrophic scars. *Biomaterials* **2016**, 83 (83), 169–181.
- (18) Ding, J.; Zhang, J.; Li, J.; Li, D.; Xiao, C.; Xiao, H.; Yang, H.; Zhuang, X.; Chen, X. Electrospun polymer biomaterials. *Prog. Polym. Sci.* **2019**, *90*, 1–34.
- (19) Sridhar, R.; Lakshminarayanan, R.; Madhaiyan, K.; Amutha Barathi, V.; Lim, K. H. C.; Ramakrishna, S. Electrosprayed nanoparticles and electrospun nanofibers based on natural materials: applications in tissue regeneration, drug delivery and pharmaceuticals. *Chem. Soc. Rev.* **2015**, *44* (3), 790–814.
- (20) Zhang, L.; Yu, W.; Han, C.; Guo, J.; Zhang, Q.; Xie, H.; Shao, Q.; Sun, Z.; Guo, Z. Large Scaled Synthesis of Heterostructured Electrospun TiO2/SnO2 Nanofibers with an Enhanced Photocatalytic Activity. *J. Electrochem. Soc.* **2017**, *164* (9), H651.
- (21) Huang, J.; Cao, Y.; Shao, Q.; Peng, X.; Guo, Z. Magnetic Nanocarbon Adsorbents with Enhanced Hexavalent Chromium Removal: Morphology Dependence of Fibrillar vs Particulate Structures. *Ind. Eng. Chem. Res.* **2017**, *56* (38), 10689–10701.
- (22) Guo, Y.; Xu, G.; Yang, X.; Ruan, K.; Ma, T.; Zhang, Q.; Gu, J.; Wu, Y.; Liu, H.; Guo, Z. Significantly enhanced and precisely modeled thermal conductivity in polyimide nanocomposites with chemically modified graphene via in situ polymerization and electrospinning-hot press technology. *J. Mater. Chem. C* **2018**, *6* (12), 3004–3015.
- (23) Guo, Y.; Yang, X.; Ruan, K.; Kong, J.; Dong, M.; Zhang, J.; Gu, J.; Guo, Z. ReducedGraphene Oxide Heterostructured Silver Nanoparticles Significantly Enhanced Thermal Conductivities in Hot-Pressed Electrospun Polyimide Nanocomposites. ACS Appl. Mater. Interfaces 2019, 11 (28), 25465–25473.
- (24) Li, Y.; Zhou, B.; Zheng, G.; Liu, X.; Li, T.; Yan, C.; Cheng, C.; Dai, K.; Liu, C.; Shen, C.; Guo, Z. Continuously prepared highly conductive and stretchable SWNT/MWNT synergistically composited electrospun thermoplastic polyurethane yarns for wearable sensing. *J. Mater. Chem. C* **2018**, 6 (9), 2258–2269.
- (25) Wu, J.; Li, Y.; He, C.; Kang, J.; Ye, J.; Xiao, Z.; Zhu, J.; Chen, A.; Feng, S.; Li, X.; Xiao, J.; Xian, M.; Wang, Q. Novel H2S Releasing Nanofibrous Coating for In Vivo Dermal Wound Regeneration. *ACS Appl. Mater. Interfaces* **2016**, 8 (41), 27474–27481.
- (26) Feng, S.; Zhao, Y.; Xian, M.; Wang, Q. Biological thiolstriggered hydrogen sulfide releasing microfibers for tissue engineering applications. *Acta Biomater.* **2015**, *27*, 205–213.
- (27) Rnjakkovacina, J.; Wise, S. G.; Li, Z.; Maitz, P. K. M.; Young, C. J.; Wang, Y.; Weiss, A. S. Electrospun synthetic human elastin:collagen composite scaffolds for dermal tissue engineering. *Acta Biomater.* **2012**, *8* (10), 3714–3722.

- (28) Rho, K. S.; Jeong, L.; Lee, G.; Seo, B.; Park, Y. J.; Hong, S.; Roh, S.; Cho, J. J.; Park, W. H.; Min, B. Electrospinning of collagen nanofibers: effects on the behavior of normal human keratinocytes and early-stage wound healing. *Biomaterials* **2006**, *27* (8), 1452–1461
- (29) Liang, D.; Hsiao, B. S.; Chu, B. Functional electrospun nanofibrous scaffolds for biomedical applications. *Adv. Drug Delivery Rev.* **2007**, *59* (14), 1392–412.
- (30) Edelman, E. R.; Mathiowitz, E.; Langer, R.; Klagsbrun, M. Controlled and modulated release of basic fibroblast growth factor. *Biomaterials* **1991**, *12*, 619–626.
- (31) Wang, C.; Wang, Q.; Gao, W.; Zhang, Z.; Lou, Y.; Jin, H.; Chen, X.; Lei, B.; Xu, H.; Mao, C. Highly efficient local delivery of endothelial progenitor cells significantly potentiates angiogenesis and full-thickness wound healing. *Acta Biomater.* **2018**, *69*, 156–169.
- (32) Zbinden, A.; Browne, S.; Altiok, E. I.; Svedlund, F. L.; Jackson, W. M.; Healy, K. E. Multivalent conjugates of basic fibroblast growth factor enhance in vitro proliferation and migration of endothelial cells. *Biomater. Sci.* **2018**, *6* (5), 1076–1083.
- (33) Choi, S. M.; Lee, K. M.; Kim, H. J.; Park, I. K.; Kang, H. J.; Shin, H. C.; Baek, D.; Choi, Y.; Park, K. H.; Lee, J. W. Effects of structurally stabilized EGF and bFGF on wound healing in type I and type II diabetic mice. *Acta Biomater.* **2018**, *66*, 325–334.
- (34) Lebleu, V. S.; Macdonald, B. A.; Kalluri, R. Structure and Function of Basement Membranes. *Exp. Biol. Med.* **2007**, 232 (9), 1121–1129.
- (35) Kalluri, R. Basement membranes: structure, assembly and role in tumour angiogenesis. *Nat. Rev. Cancer* **2003**, *3* (6), 422–433.
- (36) Ingber, D. E.; Folkman, J. Mechanochemical switching between growth and differentiation during fibroblast growth factor-stimulated angiogenesis in vitro: role of extracellular matrix. *J. Cell Biol.* **1989**, 109 (1), 317–330.
- (37) Gates, E. D. H.; Lin, J. S.; Weinberg, J. S.; Hamilton, J.; Prabhu, S. S.; Hazle, J. D.; Fuller, G. N.; Baladandayuthapani, V.; Fuentes, D.; Schellingerhout, D. Guiding the First Biopsy in Glioma Patients using Estimated Ki67 Maps Derived from Magnetic Resonance Imaging: Conventional versus Advanced Imaging. *Neuro-Oncology* **2019**, *21* (4), 527–536.
- (38) He, S.; Xia, T.; Wang, H.; Wei, L.; Luo, X.; Li, X. Multiple release of polyplexes of plasmids VEGF and bFGF from electrospun fibrous scaffolds towards regeneration of mature blood vessels. *Acta Biomater.* **2012**, 8 (7), 2659–69.
- (39) Wu, J.; Xiao, Z.; Chen, A.; He, H.; He, C.; Shuai, X.; Li, X.; Chen, S.; Zhang, Y.; Ren, B.; Zheng, J.; Xiao, J. Sulfated zwitterionic poly(sulfobetaine methacrylate) hydrogels promote complete skin regeneration. *Acta Biomater.* **2018**, *71*, 293–305.
- (40) He, H.; Xiao, Z.; Zhou, Y.; Chen, A.; Xuan, X.; Li, Y.; Guo, X.; Zheng, J.; Xiao, J.; Wu, J. Zwitterionic poly(sulfobetaine methacrylate) hydrogels with optimal mechanical properties for improving wound healing in vivo. *J. Mater. Chem. B* **2019**, *7* (10), 1697–1707.
- (41) Wu, J.; Chen, A.; Zhou, Y.; Zheng, S.; Yang, Y.; An, Y.; Xu, K.; He, H.; Kang, J.; Luckanagul, J. A.; Xian, M.; Xiao, J.; Wang, Q. Novel H2S-Releasing hydrogel for wound repair via in situ polarization of M2 macrophages. *Biomaterials* **2019**, 222, 119398.